

Exact large deviations and emergent long-range correlations in sequential quantum East circuits

Jimin Li,^{1,*} Bruno Bertini,² Juan P. Garrahan,^{3,4} and Robert L. Jack^{1,5}

¹*Department of Applied Mathematics and Theoretical Physics, University of Cambridge, Wilberforce Road, Cambridge CB3 0WA, United Kingdom*

²*School of Physics and Astronomy, University of Birmingham, Birmingham B15 2TT, United Kingdom*

³*School of Physics and Astronomy, University of Nottingham, Nottingham, NG7 2RD, UK*

⁴*Centre for the Mathematics and Theoretical Physics of Quantum Non-Equilibrium Systems, University of Nottingham, Nottingham, NG7 2RD, UK*

⁵*Yusuf Hamied Department of Chemistry, University of Cambridge, Lensfield Road, Cambridge CB2 1EW, United Kingdom*

(Dated: September 10, 2025)

Exploiting quantum measurements is a promising route for preparation of correlated quantum states. We use methods from large deviation theory to solve this problem exactly for a specific system: the deterministic quantum East circuit with boundary measurements. We show that conditioning on measurement outcomes generates a long-range correlated state, despite typical trajectories being trivial. We derive the channel that optimally realizes the rare measurement trajectories, and establish a formal connection with the Petz recovery (time-reversal) map. We compute one- and two-point correlation functions in the conditioned state, revealing finite two-body correlations at arbitrarily large separations, and an underlying fractal structure, related to the Sierpiński triangle. These results demonstrate explicitly how boundary measurements can be used to control bulk properties of a quantum system.

Introduction – The current decade has witnessed the rise of quantum circuits—quantum many-body systems in discrete space and discrete time—as a new paradigm to understand out-of-equilibrium quantum matter [1–3]. In broad terms, this has occurred for three main reasons: (i) in circuit systems one can discard much unnecessary detail while maintaining only essential physical ingredients, such as the locality of interactions; (ii) the symmetry between space and time realised by quantum circuits offers more avenues for theoretical analysis of their dynamics [1–3]; and (iii) circuits do model accurately certain actual quantum devices [4–8].

A particularly significant research direction facilitated by the discrete spacetime setting, has been the interplay of unitary dynamics and measurements. This raises both conceptual and practical questions for quantum dynamics and quantum computation: measurements can tame the growth of entanglement induced by unitary evolution, leading to much-studied phase transitions in conditioned states, see e.g. Refs. [9, 10]; combining unitary dynamics and measurements can also allow for the preparation of highly entangled states at low circuit depths, see e.g. Refs. [11–15] and references therein.

A convenient setting for such investigations is based on so-called “collision models” [16–23] (a discrete time version of the input-output formalism [24–26]). Here, a quantum system is made to interact with a different ancilla at every step of the evolution, after which the ancilla is measured. Like other versions of quantum Markov chains, a collision model defines a quantum channel for the dynamics of the average state; it also yields

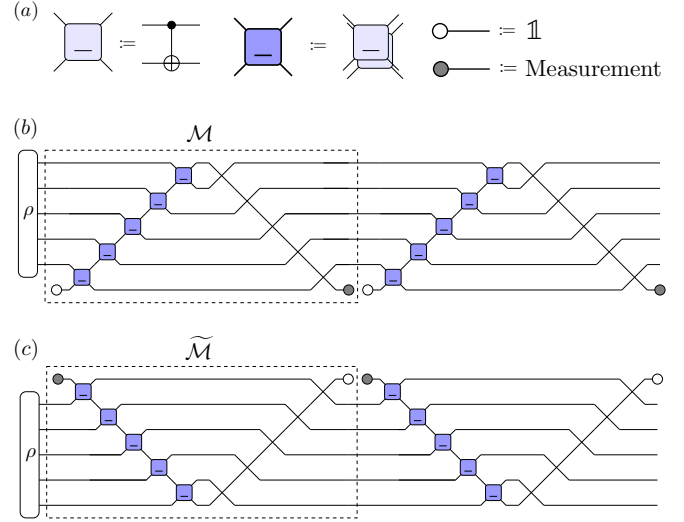


FIG. 1. Sequential quantum East circuits. (a) CNOT gate, its folded counterpart, and identity and (diagonal) measurement matrices. (b) Sequential East circuit consisting of two iterations of the channel \mathcal{M} . The circuit acts on $L + 1$ sites ($L = 5$ in the figure), which couple an input on the first L sites to a maximally mixed ancilla. Measurements are performed at the ancilla. (c) Alternative circuit in which the ancilla is prepared in a non-trivial mixed state and traced after each application of the channel $\tilde{\mathcal{M}}$.

an *unravelling* into quantum trajectories for the stochastic evolution of the state conditioned on the measurements [26–28]. Specifically, given the channel that defines the stochastic dynamics, the statistics of measurements and conditioned states are encoded by the *tilted channel* [29–31]. This works as follows: the outcomes of

* j1939@cam.ac.uk

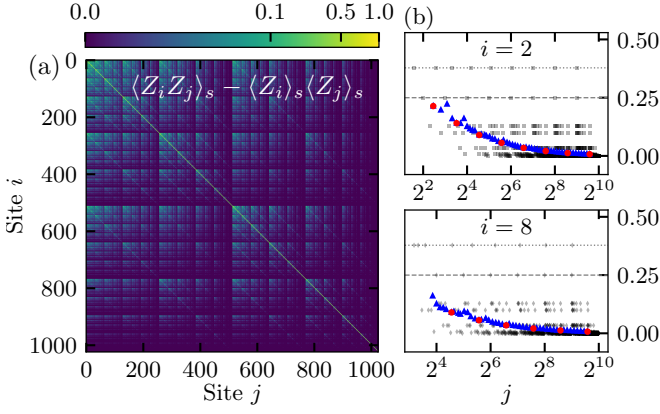


FIG. 3. (a) Correlation function $C_s(i, j)$ for $s = 0.9$ and $L = 1024$. (b) $C_s(i, j)$ as a function of $j > i$ for fixed $i = 2$ (top) and $i = 8$ (bottom). The gray dashed and dotted horizontal lines indicate the values of $C_s(2^m, 2^n)$ and $C_s(2^m, 2^n + 2^m)$. The red circles are the averages $[C_s(i, \cdot)]_{2^{(n/8)+1}}$. The blue triangles are $[C_s(i, \cdot)]_{2^{(n/8)}}$.

as a matrix, $\widetilde{\mathcal{M}}_s$ has a special structure: its spectrum is $\{0, 1\}$, the eigenvalue 1 is non-degenerate, and the largest Jordan block corresponding to the eigenvalue 0 has size L . In fact an even stronger fact holds [38]: as long as we use tilting matrices of the form Eq. (1) the same structure is found for all s . This means that even when considering different tilt parameters $(s_1 \cdots s_t)$ at each time step t , the state at time $t \geq L$ is given by a form similar to that of Eq. (5),

$$\rho_{t \geq L} = \widetilde{\mathcal{M}}_{s_t} [\cdots \widetilde{\mathcal{M}}_{s_1} [\rho_0]] = \mathcal{U}^\dagger(m_{s_t} \otimes \cdots \otimes m_{s_{t-L+1}}) e^{-\sum_{t'=t-L+1}^t \theta(s_{t'})}, \quad (15)$$

which is independent of the initial condition ρ_0 . This means that after L steps this process loses all memory of the initial condition and only retains information of the last L tilt matrices.

Long-ranged correlations in the conditioned state – We now show that in contrast to the trivial stationary state of \mathcal{M} , when conditioning on measurements, the state develops long range correlations. Consider a system operator O . Its expectation value at some intermediate time t over post-selected trajectories that run between times 0 and T can be obtained from the tilted channel as [29, 32]

$$\langle O(t) \rangle_s := \frac{\text{Tr}(\mathcal{M}_s^{T-t} [\mathcal{O} \mathcal{M}_s^t [\rho_0]])}{\text{Tr}(\mathcal{M}_s^T [\rho_0])}. \quad (16)$$

In the limit of long times ($t, T \rightarrow \infty$) we can use the fixed point structure, Eqs. (3-5), to obtain at stationarity

$$\langle O \rangle_s = \text{Tr}[\mathcal{U}^\dagger(O) m_s^{\otimes L}] e^{-L\theta(s)}. \quad (17)$$

Given the finite convergence time of the circuit, cf. Eq. (15), the above expression actually holds for any $L \leq t \leq T - L$. Also, due to Eq. (14), these are also the steady state correlations of the circuit $\widetilde{\mathcal{M}}_s$.

Consider the operator Z_i that acts as Pauli σ^z on site i and trivially on all other sites. One can show [38] (where we label sites $i = 0, \dots, L - 1$)

$$\tilde{Z}_i := \mathcal{U}^\dagger(Z_i) = \prod_{k=0}^i Z_k^{\beta_{i,k}}, \quad (18)$$

where $\beta_{i,k} = \binom{i}{k} \bmod 2$ is the Sierpiński triangle. With Eq. (18), using Eq. (17) we can calculate the one- and two-point correlations of Z_i ,

$$\langle Z_i \rangle_s = \exp \left[q(s) \sum_{k=0}^i \beta_{i,k} \right], \quad (19)$$

$$\langle Z_i Z_j \rangle_s = \exp \left\{ q(s) \left[\sum_{k=0}^i (\beta_{i,k} \oplus \beta_{j,k}) + \sum_{k=i+1}^j \beta_{j,k} \right] \right\}, \quad (20)$$

where we consider $i < j$, $s > 0$, we have defined $\beta \oplus \beta' = (\beta + \beta') \bmod 2$, and $q(s) = \ln \tanh(s)$. For $s < 0$ the same formulae hold but q is complex [$\text{Im}(q) = \pi$]. Therefore, while the expectation values are still real they can be negative. For $s \rightarrow 0$, $\text{Re}(q) \rightarrow -\infty$ and the expectation values above vanish (except for $i = j$), reflecting that $\rho_s^\dagger \rightarrow \mathbb{1}$ in this limit. In the limit $s \rightarrow \infty$ we have $q(s) \rightarrow 0$ and both expectation values approach one reflecting that $\rho_s^\dagger \rightarrow |0\rangle\langle 0|^{\otimes L}$.

The result for $\langle Z_i \rangle_s$ means that the system has no “bulk”, i.e., far from the origin, this one-point function is close to zero at most sites, but there are some special sites where it stays of order unity: for example, $\langle Z_i \rangle_s = e^{2q(s)}$ for $i = 2^m$.

To understand the “typical” behaviour of the correlators, we average them over spatial windows, as follows. Recalling Eq. (19) we consider $V_j = \sum_{k=0}^j \beta_{j,k}$ which is the number of 1’s in the j th row of the Sierpiński’s triangle. We take $L = 2^m$ and average the k th power of V_j over rows j between 0 and $L - 1$ to obtain [38]

$$[V^k]_0^L = \left(\frac{1 + 2^k}{2} \right)^m = L^{d_f(k)-1} \quad (21)$$

where $[(\cdot)]_a^b := (b - a)^{-1} \sum_{j=a}^{b-1} (\cdot)_j$ is the windowed average, and $d_f(k) := \ln(1 + 2^k) / \ln 2$ [$d_f(1) \approx 1.584$ is the fractal dimension of the Sierpiński triangle]. This gives the following averaged one-point function

$$[\langle Z \rangle_s]_0^L = \frac{1}{2^m} \sum_{j=0}^m \binom{m}{j} e^{2^j q(s)} \geq \frac{e^{q(s)}}{L}. \quad (22)$$

A similar fractal structure is also observed in the connected two-point function

$$C_s(i, j) = \langle Z_i Z_j \rangle_s - \langle Z_i \rangle_s \langle Z_j \rangle_s. \quad (23)$$

For instance, Fig. 3 shows that there exist pairs of sites with arbitrarily large separation with C_s of the order unity, indicating infinite-ranged correlations. From

Eq. (20) we have that for positive integers $m \neq n$

$$C_s(2^m, 2^n) = e^{2q(s)} - e^{4q(s)} \quad (24)$$

$$C_s(2^m, 2^n + 2^m) = e^{2q(s)} - e^{6q(s)} \quad (25)$$

which do not decay as m, n increase, see Fig 3.

On the other hand, taking $i = 2^m$ and averaging j in the window $[2^n, 2^{n+1} - 1]$ with $n > m$ we find [38]

$$[C_s(2^m, \cdot)]_{2^n}^{2^{n+1}} = \frac{1}{2^n} \sum_{j=0}^{n-1} \binom{n-1}{j} \left(e^{2^{j+2}q(s)} - 2 \sinh[2q(s)] e^{2^{j+1}q(s)} \right) + \frac{e^{2(2^n+1)q(s)}}{2^n}. \quad (26)$$

This average provides an estimate of the typical correlations in the conditioned state of Eq. (5), see Fig. 3. These spatially averaged correlations decay algebraically with the window size (which is 2^n); they are independent of m so this two-body correlation is primarily determined by the absolute distance from the origin and not the distance between the qubits. We note that while ρ_s^Δ has long-ranged correlations, these are classical in nature as the state is separable (it is diagonal in the computational basis).

Discussion – Here we have calculated exactly the dynamical large deviations of measurements at the boundary of a sequential quantum East circuit. Despite the fact that the stationary state is trivial and the measurements a Bernoulli process, we have shown that when the final state is conditioned (specifically, exponentially tilted) on the measurement outcomes it contains long-range correlations. This is a form of boundary-bulk correspondence,

where measurements on the boundary control the structure on the bulk of the system. Our result here is one of the very few examples of an exact characterisation of dynamical large deviations in a genuine many-body system.

We have also found an interesting connection to time-reversal, where the “Doob dynamics” that optimally samples the rare events of the circuit corresponds to the Petz recovery map that time-reverses the dynamics of a different circuit whose environment is structured. As for the large deviations, this result is a rare example of the exact solution of a Petz map in a many-body problem.

The circuit we study can be realised in current quantum devices as it requires only CNOT and SWAP gates together with mid-circuit measurements [42]. Our results provide a way to create long-range correlated states simply by controlling a boundary ancilla. Being exact, our results can also serve as a benchmark for experimental devices. While the correlations we have shown here are only classical, a similar setting could be used to generate genuine entanglement by simply rotating the measurement basis. We hope to report on this and other extensions in future work.

ACKNOWLEDGMENTS

JL acknowledges support by the UKRI Grant No. EP/Z003342/1. BB acknowledges financial support from the Royal Society through the University Research Fellowship No. 201101. JPG acknowledges financial support from EPSRC Grant No. EP/V031201/1 and Leverhulme Trust Grant No. RPG-2024-112.

-
- [1] A. C. Potter and R. Vasseur, Entanglement Dynamics in Hybrid Quantum Circuits, in *Entanglement in Spin Chains: From Theory to Quantum Technology Applications*, edited by A. Bayat, S. Bose, and H. Johannesson (Cham, 2022) pp. 211–249.
 - [2] M. P. Fisher, V. Khemani, A. Nahum, and S. Vijay, Random quantum circuits, *Annu. Rev. Condens. Matter Phys.* **14**, 335 (2023).
 - [3] B. Bertini, P. W. Claeys, and T. Prosen, Exactly solvable many-body dynamics from space-time duality, *arXiv:2505.11489* (2025).
 - [4] S. J. Evered, D. Bluvstein, M. Kalinowski, S. Ebadi, T. Manovitz, H. Zhou, S. H. Li, A. A. Geim, T. T. Wang, N. Maskara, *et al.*, High-fidelity parallel entangling gates on a neutral-atom quantum computer, *Nature* **622**, 268 (2023).
 - [5] J.-S. Chen, E. Nielsen, M. Ebert, V. Inlek, K. Wright, V. Chaplin, A. Maksymov, E. Pérez, A. Poudel, P. Maunz, and J. Gamble, Benchmarking a trapped-ion quantum computer with 30 qubits, *Quantum* **8**, 1516 (2024).
 - [6] C. M. Löschner, J. M. Toba, A. C. Hughes, S. A. King, M. A. Weber, R. Srinivas, R. Matt, R. Nourshargh, D. T. C. Allcock, C. J. Ballance, C. Matthiesen, M. Malinowski, and T. P. Harty, Scalable, high-fidelity all-electronic control of trapped-ion qubits, *arXiv:2407.07694* (2024).
 - [7] L. E. Fischer, M. Leahy, A. Eddins, N. Keenan, D. Ferracin, M. A. C. Rossi, Y. Kim, A. He, F. Pietracaprina, B. Sokolov, S. Dooley, Z. Zimborás, F. Tacchino, S. Maniscalco, J. Goold, G. García-Pérez, I. Tavernelli, A. Kandala, and S. N. Filippov, Dynamical simulations of many-body quantum chaos on a quantum computer, *arXiv:2411.00765* (2024).
 - [8] R. Acharya, D. A. Abanin, L. Aghababaie-Beni, I. Aleiner, T. I. Andersen, *et al.*, Quantum error correction below the surface code threshold, *Nature* **638**, 920 (2025).
 - [9] B. Skinner, J. Ruhman, and A. Nahum, Measurement-Induced Phase Transitions in the Dynamics of Entanglement, *Phys. Rev. X* **9**, 031009 (2019).
 - [10] Y. Li, X. Chen, and M. P. A. Fisher, Measurement-driven entanglement transition in hybrid quantum circuits, *Phys. Rev. B* **100**, 134306 (2019).
 - [11] L. Piroli, G. Styliaris, and J. I. Cirac, Quantum Circuits Assisted by Local Operations and Classical Communication: Transformations and Phases of Matter, *Phys. Rev.*

- Lett.* **127**, 220503 (2021).
- [12] G.-Y. Zhu, N. Tantivasadakarn, A. Vishwanath, S. Trebst, and R. Verresen, Nishimori's Cat: Stable Long-Range Entanglement from Finite-Depth Unitaries and Weak Measurements, *Phys. Rev. Lett.* **131**, 200201 (2023).
 - [13] M. Iqbal, N. Tantivasadakarn, T. M. Gatterman, J. A. Gerber, K. Gilmore, D. Gresh, A. Hankin, N. Hewitt, C. V. Horst, M. Matheny, *et al.*, Topological order from measurements and feed-forward on a trapped ion quantum computer, *Commun. Phys.* **7**, 205 (2024).
 - [14] S. Gopalakrishnan, Push-down automata as sequential generators of highly entangled states, *arXiv:2305.04951* (2023).
 - [15] T.-C. Lu, S. Gopalakrishnan, and Y. You, Spacetime duality between sequential and measurement-feedback circuits, *arXiv:2507.12523* (2025).
 - [16] F. Ciccarello, S. Lorenzo, V. Giovannetti, and G. M. Palma, Quantum collision models: Open system dynamics from repeated interactions, *Phys. Rep.* **954**, 1 (2022).
 - [17] D. Cilluffo, G. Buonaiuto, I. Lesanovsky, A. Carollo, S. Lorenzo, G. M. Palma, F. Ciccarello, and F. Carollo, Microscopic biasing of discrete-time quantum trajectories, *Quantum Sci. Technol.* **6**, 045011 (2021).
 - [18] M. Cech, I. Lesanovsky, and F. Carollo, Thermodynamics of Quantum Trajectories on a Quantum Computer, *Phys. Rev. Lett.* **131**, 120401 (2023).
 - [19] M. Cech, M. Cea, M. C. Bañuls, I. Lesanovsky, and F. Carollo, Space-Time Correlations in Monitored Kinetically Constrained Discrete-Time Quantum Dynamics, *Phys. Rev. Lett.* **134**, 230403 (2025).
 - [20] C. Schön, E. Solano, F. Verstraete, J. I. Cirac, and M. M. Wolf, Sequential Generation of Entangled Multiqubit States, *Phys. Rev. Lett.* **95**, 110503 (2005).
 - [21] C. Schön, K. Hammerer, M. M. Wolf, J. I. Cirac, and E. Solano, Sequential generation of matrix-product states in cavity QED, *Phys. Rev. A* **75**, 032311 (2007).
 - [22] M. C. Bañuls, D. Pérez-García, M. M. Wolf, F. Verstraete, and J. I. Cirac, Sequentially generated states for the study of two-dimensional systems, *Phys. Rev. A* **77**, 052306 (2008).
 - [23] Z.-Y. Wei, D. Malz, and J. I. Cirac, Sequential Generation of Projected Entangled-Pair States, *Phys. Rev. Lett.* **128**, 010607 (2022).
 - [24] V. Belavkin, A stochastic posterior Schrödinger equation for counting nondemolition measurement, *Lett. Math. Phys.* **20**, 85 (1990).
 - [25] H. Carmichael, *An open systems approach to quantum optics* (1993).
 - [26] C. Gardiner and P. Zoller, *Quantum noise* (Berlin, Heidelberg, 2004).
 - [27] M. B. Plenio and P. L. Knight, The quantum-jump approach to dissipative dynamics in quantum optics, *Rev. Mod. Phys.* **70**, 101 (1998).
 - [28] H. P. Breuer and F. Petruccione, *The theory of open quantum systems* (Great Clarendon Street, 2002).
 - [29] J. P. Garrahan and I. Lesanovsky, Thermodynamics of Quantum Jump Trajectories, *Phys. Rev. Lett.* **104**, 160601 (2010).
 - [30] M. Esposito, U. Harbola, and S. Mukamel, Nonequilibrium fluctuations, fluctuation theorems, and counting statistics in quantum systems, *Rev. Mod. Phys.* **81**, 1665 (2009).
 - [31] J. P. Garrahan, Aspects of non-equilibrium in classical and quantum systems: Slow relaxation and glasses, dynamical large deviations, quantum non-ergodicity, and open quantum dynamics, *Physica A* **504**, 130 (2018).
 - [32] F. Carollo, J. P. Garrahan, I. Lesanovsky, and C. Pérez-Espigares, Making rare events typical in Markovian open quantum systems, *Phys. Rev. A* **98**, 010103 (2018).
 - [33] D. Berenstein and J. Zhao, Exotic equilibration dynamics on a 1-D quantum CNOT gate lattice, *arXiv:2102.05745* (2021).
 - [34] K. Klobas, C. De Fazio, and J. P. Garrahan, Exact pre-transition effects in kinetically constrained circuits: Dynamical fluctuations in the Floquet-East model, *Phys. Rev. E* **110**, L022101 (2024).
 - [35] B. Bertini, P. Kos, and T. Prosen, Localized Dynamics in the Floquet Quantum East Model, *Phys. Rev. Lett.* **132**, 080401 (2024).
 - [36] B. Bertini, C. De Fazio, J. P. Garrahan, and K. Klobas, Exact quench dynamics of the Floquet quantum East model at the deterministic point, *Phys. Rev. Lett.* **132**, 120402 (2024).
 - [37] F. Carollo, R. L. Jack, and J. P. Garrahan, Unraveling the Large Deviation Statistics of Markovian Open Quantum Systems, *Phys. Rev. Lett.* **122**, 130605 (2019).
 - [38] See Supplemental Material at [URL] for more details.
 - [39] D. Petz, Sufficient subalgebras and the relative entropy of states of a von Neumann algebra, *Comm. Math. Phys.* **105**, 123 (1986).
 - [40] H. Kwon, R. Mukherjee, and M. S. Kim, Reversing Lindblad Dynamics via Continuous Petz Recovery Map, *Phys. Rev. Lett.* **128**, 020403 (2022).
 - [41] G. Bai, F. Buscemi, and V. Scarani, Quantum Bayes' rule and Petz transpose map from the minimum change principle, *arXiv:2410.00319* (2025).
 - [42] K. Rudinger, G. J. Ribeill, L. C. G. Govia, M. Ware, E. Nielsen, K. Young, T. A. Ohki, R. Blume-Kohout, and T. Proctor, Characterizing mid-circuit measurements on a superconducting qubit using gate set tomography, *arXiv:2103.03008* (2021).
 - [43] B. Bertini, C. D. Fazio, J. P. Garrahan, and K. Klobas, Exact quench dynamics of the Floquet quantum East model at the deterministic point, *arXiv:2310.06128* (2023).
 - [44] L. Piroli and J. I. Cirac, Quantum Cellular Automata, Tensor Networks, and Area Laws, *Phys. Rev. Lett.* **125**, 190402 (2020).
 - [45] M. A. Nielsen and I. L. Chuang, *Quantum computation and quantum information* (Shaftesbury Road, 2010).
 - [46] H. Touchette, Introduction to dynamical large deviations of Markov processes, *Physica A* **504**, 5 (2018).
 - [47] R. L. Jack, Ergodicity and large deviations in physical systems with stochastic dynamics, *Eur. Phys. J. B* **93**, 74 (2020).
 - [48] J. Li, R. L. Jack, B. Bertini, and J. P. Garrahan, Efficient post-selection in light cone correlations of monitored quantum circuits, *Phys. Rev. B* **111**, 024309 (2025).
 - [49] S. Gopalakrishnan and A. Lamacraft, Unitary circuits of finite depth and infinite width from quantum channels, *Phys. Rev. B* **100**, 064309 (2019).
 - [50] G. Giudice, G. Giudici, M. Sonner, J. Thoenness, A. Leroise, D. A. Abanin, and L. Piroli, Temporal entanglement, quasiparticles and the role of interactions, *Phys. Rev. Lett.* **128**, 220401 (2022).
 - [51] V. Popkov, G. M. Schütz, and D. Simon, ASEP on a ring conditioned on enhanced flux, *J. Stat. Mech.: Theory*

- Exp. **2010** (10), P10007.
- [52] R. L. Jack, I. R. Thompson, and P. Sollich, Hyperuniformity and Phase Separation in Biased Ensembles of Trajectories for Diffusive Systems, *Phys. Rev. Lett.* **114**, 060601 (2015).

Supplemental Material: Exact large deviations and emergent long-range correlations in sequential quantum East circuits

In this supplemental material, we provide the following to complement the main text:

- In Sec. **I**, we provide the detailed definitions of the circuits of interest, and the standard diagrammatic notions.
- In Sec. **II**, we review the applications of Level-1 large deviation methods to quantum operations.
- In Sec. **III**, we discuss the tilted quantum channel and show the exact dominant eigenmatrices.
- In Sec. **IV**, we discuss the quantum Doob transformation.
- In Sec. **V**, we provide of the details of time-inhomogeneous tilting setup.
- In Sec. **VI**, we provide the calculations of observables in the conditioned state.

I. QUANTUM EAST CIRCUITS

In this section, we introduce the quantum East circuits studied in the main text, which consist of sequential quantum circuits with boundary measurement, and summarise the standard graphical notations for quantum circuits.

A. Sequential quantum circuits with boundary measurement

Throughout this work, we focus on $(1+1)$ -dimensional quantum circuits that consist of qubits with a local Hilbert space of $\mathcal{H}_i = \mathbb{C}^2$, where the subscript i labels the site index. The building block of circuits we are considering is the CNOT gate,

$$U^{\text{CNOT}} = P^0 \otimes \mathbf{1} + P^1 \otimes X, \quad (\text{SM-1})$$

where $\{X, Y, Z\}$ are the spin- $\frac{1}{2}$ Pauli matrices, and $P^0 = (\mathbf{1} + Z)/2$ and $P^1 = (\mathbf{1} - Z)/2$ are the projection operators in the computational basis. To make a connection with previous work on the quantum East circuits, the gate considered in Ref [43] is

$(X \otimes X) U^{\text{SWAP}} U^{\text{CNOT}} U^{\text{SWAP}} (X \otimes X) = \mathbf{1} \otimes P^1 + X \otimes P^0$, where U^{SWAP} is the SWAP gate.

A *sequential quantum circuit (SQC)* is a special kind of linear-depth quantum circuit, where every layer only consists of non-identity gates on a sub-region of the domain [20–23]. Each layer of the SQC considered in this work consists of either a single CNOT gate $U_{i,i+1}^{\text{CNOT}}$ acting on the i and $i+1$ sites, or a similar SWAP gate $U_{i,i+1}^{\text{SWAP}}$.

The circuit is defined by applying a sequence of CNOT gates as

$$U_{\text{SQC}} := U_{0,1}^{\text{CNOT}} U_{1,2}^{\text{CNOT}} \cdots U_{L-1,L}^{\text{CNOT}} \quad (\text{SM-2})$$

we also define an operator

$$W_{\text{SQC}} := U_{L-1,L}^{\text{SWAP}} U_{L-2,L-1}^{\text{SWAP}} \cdots U_{0,1}^{\text{SWAP}} \quad (\text{SM-3})$$

which realises the *shift* operation on $L+1$ sites [44].

The system considered in Fig. 1(b) has L qubits and describes the following dynamics. Starting with a system density matrix $\rho \in \text{End}(\mathcal{H}^L \otimes \mathcal{H}^L)$, we first couple the system to an ancilla qubit in the maximally mixed state; second, apply the sequential circuit; third, measure the ancilla in the computational basis. The (un-normalised) conditional state of the system associated with measurement outcome $k = 0, 1$ is then

$$\text{Tr}_L \left[P_L^{(k)} \mathcal{W}_{\text{SQC}} \circ \mathcal{U}_{\text{SQC}}(\rho \otimes \mathbb{1}) \right], \quad (\text{SM-4})$$

where $P_L^{(k)} = \mathbb{1} \otimes |k\rangle\langle k|$ is a projector for state $|k\rangle$ of the ancilla (which is the L th qubit); the trace is over the ancilla, and we introduced superoperators

$$\mathcal{U}_{\text{SQC}}(\cdot) = U_{\text{SQC}}(\cdot) U_{\text{SQC}}^\dagger, \quad \mathcal{W}_{\text{SQC}}(\cdot) = W_{\text{SQC}}(\cdot) W_{\text{SQC}}^\dagger. \quad (\text{SM-5})$$

To define the channel \mathcal{M} we average over measurement outcomes to obtain

$$\mathcal{M}[\rho] := \text{Tr}_L \left[\mathcal{W}_{\text{SQC}} \circ \mathcal{U}_{\text{SQC}}(\rho \otimes \mathbb{1}) \right], \quad (\text{SM-6})$$

This quantum channel \mathcal{M} is a *completely positive and trace preserving* (CPTP) linear map [45], note that $\mathcal{M}^\dagger[\mathbb{1}] = \mathbb{1}$. Additionally, we observe that $\mathcal{M}[\mathbb{1}] = \mathbb{1}$, which makes the quantum channel *unital*. Unital quantum channels are quantum analogues of bistochastic matrices in classical Markov matrices.

B. Complementary channel

In addition to the SQC with boundary measurement setup, we also introduce the complementary channel of Fig. 1(b), which plays an important role when considering the quantum Doob transformation.

We define

$$\tilde{U}_{\text{SQC}} := U_{L-1,L}^{\text{CNOT}} \cdots U_{1,2}^{\text{CNOT}} U_{0,1}^{\text{CNOT}} = U_{\text{SQC}}^\dagger \quad (\text{SM-7})$$

and similarly

$$\tilde{W}_{\text{SQC}} := U_{0,1}^{\text{SWAP}} U_{1,2}^{\text{SWAP}} \cdots U_{L-1,L}^{\text{SWAP}} = W_{\text{SQC}}^\dagger \quad (\text{SM-8})$$

Defining superoperators analogous to Eq. (SM-5), we consider the dynamics of the complementary channel involves where the L -qubit system is coupled to an ancilla at position 0 in initial state $|k\rangle\langle k|$: applying the sequential circuit leaves the system in state

$$\text{Tr}_0 \left[\tilde{\mathcal{W}}_{\text{SQC}} \circ \tilde{\mathcal{U}}_{\text{SQC}}(|k\rangle\langle k| \otimes \rho) \right] \quad (\text{SM-9})$$

analogous to Eq. (SM-4). For later convenience, we assign the states of the ancilla with probabilities $e^{\pm s}/(e^s + e^{-s})$ and sum over these outcomes to obtain the complementary (CPTP) channel

$$\tilde{\mathcal{M}}_s[\rho] := \text{Tr}_0 \left[(m_s)_0 \tilde{\mathcal{W}}_{\text{SQC}} \circ \tilde{\mathcal{U}}_{\text{SQC}}(\mathbb{1} \otimes \rho) \right] \frac{1}{e^s + e^{-s}} \quad (\text{SM-10})$$

where the operator $(m_s)_0 = P_0^{(0)}e^s + P_0^{(1)}e^{-s}$ acts on the ancilla, the subscript indicates that this is the zeroth qubit in this case.

C. Diagrammatic representation

We introduce the standard diagrammatic representation of quantum circuits. The CNOT and SWAP gates are represented (in the unfolded representation) as

$$U^{\text{CNOT}} = \begin{array}{c} \diagup \quad \diagdown \\ \boxed{\quad | \quad} \\ \diagdown \quad \diagup \end{array} \quad \text{and} \quad U^{\text{SWAP}} = \begin{array}{c} \diagup \quad \diagdown \\ \diagdown \quad \diagup \end{array}, \quad (\text{SM-11})$$

Moreover, U^{CNOT} is both Hermitian and unitary so $(U^{\text{CNOT}})^2 = \mathbb{1}$, that is

$$\begin{array}{c} \diagup \quad \diagdown \\ \boxed{\quad | \quad} \\ \diagdown \quad \diagup \\ \diagup \quad \diagdown \\ \boxed{\quad | \quad} \\ \diagdown \quad \diagup \end{array} = \begin{array}{c} | \\ | \end{array}. \quad (\text{SM-12})$$

The operators defined by Eqs. (SM-2, SM-7) are represented by

$$U_{\text{SQC}} = \begin{array}{c} \text{Diagram: A sequence of three square blocks connected by dashed lines. The first block is at } i=0, \text{ the second at } i=1, \text{ and the third at } i=L. \end{array} \quad \text{and} \quad \tilde{U}_{\text{SQC}} = \begin{array}{c} \text{Diagram: A sequence of three square blocks connected by dashed lines. The first block is at } i=0, \text{ the second at } i=1, \text{ and the third at } i=L. \end{array} \quad (\text{SM-13})$$

For a compact notation of quantum channels, it is convenient to work in the folded representation from quantum circuits, see e.g. Ref. [3]. To make this explicit in our notation we use a folded tensor product $\hat{\otimes}$: for example

$$\mathcal{U}^{\text{CNOT}} = U^{\text{CNOT}} \hat{\otimes} U^{\text{CNOT}} = \begin{array}{c} \text{Diagram: Two square blocks connected by a horizontal line.} \end{array} = \begin{array}{c} \text{Diagram: A single square block with four external lines.} \end{array}, \quad (\text{SM-14})$$

represents the unitary super-operator $\mathcal{U}^{\text{CNOT}}(\cdot) = U^{\text{CNOT}}(\cdot)U^{\text{CNOT}}$. Then Eq. (SM-12) is equivalent to

$$\begin{array}{c} \text{Diagram: A square block with two input circles and two output circles.} \end{array} = \begin{array}{c} \text{Diagram: A vertical line with a circle at the bottom.} \end{array} \quad \text{and} \quad \begin{array}{c} \text{Diagram: A square block with two input circles and two output circles.} \end{array} = \begin{array}{c} \text{Diagram: A vertical line with a circle at the top.} \end{array}, \quad (\text{SM-15})$$

where the empty circle is

$$|0\rangle \hat{\otimes} |0\rangle + |1\rangle \hat{\otimes} |1\rangle =: \text{Diagram: A horizontal line with a circle at the right end.} \quad (\text{SM-16})$$

As in the main text, we also introduce

$$\text{Diagram: A horizontal line with a blue circle in the middle.} := m_s := \begin{pmatrix} e^s & 0 \\ 0 & e^{-s} \end{pmatrix} \quad (\text{SM-17})$$

which we note may be alternatively represented [see Eq. (SM-10)] as

$$m_s = e^s P^{(0)} + e^{-s} P^{(1)} = e^s |0\rangle \hat{\otimes} |0\rangle + e^{-s} |1\rangle \hat{\otimes} |1\rangle \quad (\text{SM-18})$$

II. LARGE DEVIATIONS AND QUANTUM DOOB TRANSFORM

Here we review some well-established results of large deviation theory [31, 46, 47], and explain how to apply them to our SQC with measurement protocol.

The SQC is applied T times and the measurement outcomes are recorded as k_1, \dots, k_T with each k_t being either 0 or 1. Let Q_0 be the number of outcomes that are 0; also let Q_1 be the number that are 1. Clearly $Q_0 + Q_1 = T$ so the full-counting statistics is fully described by the probability distribution of $\Delta Q = (Q_1 - Q_0)$. For large times, the probability density function for $q = \Delta Q/T$ behaves as

$$\text{Prob}(q) \simeq e^{-TF(q)}, \quad (\text{SM-19})$$

where F is the rate function.

To make progress it is convenient to introduce a counting field s such that the (unnormalised) state after a measurement outcome k in Eq. (SM-4) is modified as

$$e^{(1-2k)s} \text{Tr}_L \left[P_L^{(k)} \mathcal{W}_{\text{SQC}} \circ \mathcal{U}_{\text{SQC}}(\rho \otimes \mathbb{1}) \right], \quad (\text{SM-20})$$

This means measurements with $k = 1$ are weighted by a factor e^{-s} while those with $k = 0$ are weighted by e^s . Averaging these outcomes yields the tilted channel:

$$\mathcal{M}_s[\rho] = \sum_{k=0,1} \text{Tr}_L \left[P_L^{(k)} e^{(1-2k)s} \mathcal{W}_{\text{SQC}} \circ \mathcal{U}_{\text{SQC}}(\rho \otimes \mathbb{1}) \right] \quad (\text{SM-21})$$

From Eq. (SM-18) one recognises $\sum_{k=0,1} P_L^{(k)} e^{(1-2k)s} = m_s$. Using this fact together with the diagrammatic methods of the previous section, one sees that Eq. (SM-21) is equivalent to Eq. (1) of the main text. Similarly, $\mathcal{M}_s = (e^s + e^{-s}) \widehat{\mathcal{M}}_s^\dagger$ which is Eq. (12) of the main text (here and throughout, super-operator adjoints are defined with respect to the inner product $\langle A, B \rangle = \text{Tr}[A^\dagger B]$ for operators A, B).

Note that the map \mathcal{M}_s is completely positive but not trace-preserving. Moreover, the moment generating function for ΔQ after T iterations of the map \mathcal{M}_s [starting from state ρ_0] is

$$Z(s) = \mathbb{E}[e^{-s\Delta Q}] = \text{Tr}(\mathcal{M}_s^T[\rho_0]) \quad (\text{SM-22})$$

and one sees that the growth of Z is governed by the largest eigenvalue of \mathcal{M}_s (which is guaranteed by Perron-Frobenius theory to be real and positive): for large T we have

$$Z(s) \simeq e^{T\theta(s)}, \quad (\text{SM-23})$$

with

$$\theta(s) = \ln(\max(\text{Spec}(\mathcal{M}_s))), \quad (\text{SM-24})$$

One also sees from Eq. (SM-23) that θ is the scaled cumulant generating function for the large deviations of q , which is related to its rate function by Legendre transform, as

$$\theta(s) = -\min_q [qs + F(q)], \quad F(q) = \max_\theta [-qs - \theta(s)]. \quad (\text{SM-25})$$

For ergodic channels (as considered here) the eigenmatrix of \mathcal{M}_s^\dagger associated to its dominant eigenvalue is unique and positive definite. We denote it by ℓ_s , that is

$$\mathcal{M}_s^\dagger[\ell_s] = \ell_s e^{\theta(s)} \quad (\text{SM-26})$$

This matrix can be used for the quantum Doob transformation [18, 29]: one constructs a channel as

$$\mathcal{M}_s^D[\cdot] = e^{-\theta(s)} \ell_s^{1/2} \mathcal{M}_s[\ell_s^{-1/2}(\cdot) \ell_s^{-1/2}] \ell_s^{1/2} \quad (\text{SM-27})$$

It may be verified that this channel is CPTP, in particular the trace-preserving property $(\mathcal{M}_s^D)^\dagger[\mathbb{1}] = \mathbb{1}$ is indeed satisfied. Moreover, rare trajectories of \mathcal{M} become typical for \mathcal{M}_s^D , which enables efficient post-selection [48]. It will be convenient in the following to write Eq. (SM-27) as

$$\mathcal{M}_s^D = e^{-\theta(s)} \mathcal{V}_s \circ \mathcal{M}_s \circ \mathcal{V}_s^{-1}, \quad \text{with} \quad \mathcal{V}_s(\cdot) = \ell_s^{1/2}(\cdot) \ell_s^{1/2}. \quad (\text{SM-28})$$

III. EXACT RESULTS FOR DOMINANT EIGENMATRICES

In this section, we discuss the left and right dominant eigenmatrices of the tilted channel defined in Sec. I and provide the derivations for the findings of the main text.

We focus on the tilted channel Eq. (SM-21). Unitarity of $\mathcal{W}_{\text{SQC}}, \mathcal{U}_{\text{SQC}}$ means that $\mathcal{W}_{\text{SQC}} \circ \mathcal{U}_{\text{SQC}}(\mathbb{1}) = \mathbb{1}$ [where $\mathbb{1}$ is the identity for $(L+1)$ qubits] so the right leading dominant eigenmatrix of \mathcal{M}_s can be straightforwardly seen to be the L -qubit identity:

$$\mathcal{M}_s[\mathbb{1}] = e^{\theta(s)} \mathbb{1}, \quad (\text{SM-29})$$

where the dominant eigenvalue is

$$e^{\theta(s)} = e^s + e^{-s}. \quad (\text{SM-30})$$

The left dominant eigenmatrix is more complicated, we first define the state algebraically; then we use diagrammatic methods to show that it is an eigenstate of \mathcal{M}_s^\dagger .

We define an L -qubit operator analogous to Eq. (SM-2) that only acts on qubits to the right of a given location j :

$$U_{\text{SQC}}^{(j)} := U_{j,j+1}^{\text{CNOT}} U_{j+1,j+2}^{\text{CNOT}} \cdots U_{L-2,L-1}^{\text{CNOT}} \quad (\text{SM-31})$$

such that $U_{\text{SQC}}^{(0)} = U_{\text{SQC}}$. The corresponding (folded) super-operator is $\mathcal{U}_{\text{SQC}}^{(j)} = U_{\text{SQC}}^{(j)} \hat{\otimes} U_{\text{SQC}}^{(j)}$. Finally define a super-operator

$$\mathcal{U}^\triangleleft := \mathcal{U}_{\text{SQC}}^{(L-2)} \cdots \mathcal{U}_{\text{SQC}}^{(1)} \mathcal{U}_{\text{SQC}}^{(0)} \quad (\text{SM-32})$$

Diagrammatically, this L -qubit super-operator corresponds to

$$\mathcal{U}^\triangleleft = \quad (\text{SM-33})$$

which includes a total of $L(L-1)/2$ folded CNOT gates.

Recalling the matrix m_s defined in Eq. (SM-17), we show in Sec. IIIB below that the dominant eigenmatrix of \mathcal{M}_s^\dagger is

$$\rho_s^\triangleleft = \mathcal{U}^\triangleleft (m_s^{\otimes L}), \quad (\text{SM-34})$$

that is,

$$\mathcal{M}_s^\dagger[\rho_s^\triangleleft] = e^{\theta(s)} \rho_s^\triangleleft. \quad (\text{SM-35})$$

See Eqs. (3,5) of main text. Physically, one sees that preparation of ρ_s^\triangleleft requires applying a linear-depth quantum circuit on an iterated direct product of the tilting matrix m_s . Given that m_s is diagonal and positive definite, one may also construct powers of ρ_s^\triangleleft (and its inverse), for example

$$\begin{aligned} (\rho_s^\triangleleft)^{1/2} &= \mathcal{U}^\triangleleft \left((m_s^{1/2})^{\otimes L} \right) \\ (\rho_s^\triangleleft)^{-1/2} &= \mathcal{U}^\triangleleft \left((m_s^{-1/2})^{\otimes L} \right). \end{aligned} \quad (\text{SM-36})$$

which are useful for the Doob transformation, see below.

A. Action of $\mathcal{U}^{\text{CNOT}}$ on projection operators

The operator $\mathcal{U}^{\text{CNOT}}$ acts as a permutation in the computational basis, which is useful in the following analysis. This fact can be exploited by noting how $\mathcal{U}^{\text{CNOT}}$ acts on projection operators. We first introduce the folded diagrammatic representation of projection super-operator (and operators) in the computational basis:

$$\text{---} \overset{n}{\bullet} \text{---} := \text{---} \overset{n}{\bullet} \overset{n}{\bullet} \text{---} = P^{(n)} \hat{\otimes} P^{(n)} = |n\rangle\langle n| \hat{\otimes} |n\rangle\langle n|, \quad (\text{SM-37})$$

for $n \in \{0, 1\}$. Note that Eq. (SM-18) can be written as

$$m_s = \sum_{n \in \{0,1\}} e^{s(1-2n)} \text{---} \overset{n}{\bullet} \text{---} \quad (\text{SM-38})$$

From the definition of CNOT one may readily show that

$$\begin{array}{c} \text{CNOT gate with inputs } n_1, n_2 \end{array} = \begin{array}{c} \text{CNOT gate with inputs } n_1, n_1 \oplus n_2 \end{array} \quad \text{and} \quad \begin{array}{c} \text{CNOT gate with inputs } n_1, n_2 \end{array} = \begin{array}{c} \text{CNOT gate with inputs } n_1, n_1 \end{array}, \quad (\text{SM-39})$$

Specifically, the left output of CNOT is unaffected by its right input. Combining these two relations also implies

$$\begin{array}{c} \text{CNOT gate with inputs } n_1, n_2 \text{ followed by CNOT gate with inputs } n_3, \text{left output of first CNOT} \end{array} = \begin{array}{c} \text{CNOT gate with inputs } n_1, n_2 \end{array} \quad (\text{SM-40})$$

which will be used extensively in the following.

B. Dominant eigenmatrix of \mathcal{M}_s^\dagger

To derive Eq. (SM-35) we note [by Eqs. (SM-21, SM-33, SM-34, SM-38)] that

$$\mathcal{M}_s^\dagger[\rho_s^\triangleleft] = \sum_{k, n_0, \dots, n_{L-1}} e^{\sum_i (1-2n_i)s} f^\triangleleft(k, n_0, \dots, n_{L-1}) \quad (\text{SM-41})$$

where all sums run over the set $\{0, 1\}$ and

$$f^\triangleleft(k, n_0, \dots, n_{L-1}) = \begin{array}{c} \text{Diagram showing a sequence of CNOT gates forming a ladder structure. The leftmost input is } k, \text{ and the bottom inputs are } n_0, n_{L-3}, n_{L-2}, n_{L-1}. \end{array} \quad (\text{SM-42})$$

Hence we have

$$f^{\triangleleft}(k, n_0, \dots, n_{L-1}) = \text{[Circuit Diagram]} = \text{[Simplified Circuit Diagram]} \quad (\text{SM-43})$$

where the first equality uses repeatedly Eq. (SM-39) and the second uses Eq. (SM-40) repeatedly to remove L gates and then uses again Eq. (SM-39); black dots without labels refer to projection operators on states whose specific value is not needed for the derivation. Plugging this last result back into Eq. (SM-41), the sums can be performed and the result is exactly Eq. (SM-35).

This diagrammatic computation somewhat resembles those of Refs. [49, 50] but the results here are different and rely on specific properties of CNOT gates.

IV. QUANTUM DOOB TRANSFORMATION

Using Eq. (SM-28) for the Doob transform of $\tilde{\mathcal{M}}_s$ together with Eq. (SM-35), we identify $\mathcal{V}_s(\cdot) = (\rho_s^{\triangleleft})^{1/2}(\cdot)(\rho_s^{\triangleleft})^{1/2}$ and so

$$\mathcal{V}_s = e^{-L\theta(s)} \mathcal{U}^{\triangleleft} \circ (m_s^{1/2} \hat{\otimes} m_s^{1/2})^{\otimes L} \circ \mathcal{U}^{\triangleleft}. \quad (\text{SM-44})$$

Similarly $\mathcal{V}_s^{-1} = e^{L\theta(s)} \mathcal{U}^{\triangleleft} \circ (m_s^{-1/2} \hat{\otimes} m_s^{-1/2})^{\otimes L} \circ \mathcal{U}^{\triangleleft}$. This allows \mathcal{M}_s^{D} to be constructed as in Fig. 2 of the main text, leading to a linear-depth quantum circuit. Explicitly writing

$$\mathcal{M}_s^{\text{D}} = e^{-\theta(s)} \mathcal{U}^{\triangleleft} \circ (m_s^{1/2} \hat{\otimes} m_s^{1/2})^{\otimes L} \circ \mathcal{U}^{\triangleleft} \circ \mathcal{M}_s \circ \mathcal{U}^{\triangleleft} \circ (m_s^{-1/2} \hat{\otimes} m_s^{-1/2})^{\otimes L} \circ \mathcal{U}^{\triangleleft} \quad (\text{SM-45})$$

shows the presence of four $\mathcal{U}^{\triangleleft}$'s (triangles) as well as L instances of $(m_s^{1/2} \hat{\otimes} m_s^{1/2})$ and L of $(m_s^{-1/2} \hat{\otimes} m_s^{-1/2})$.

Since $\mathcal{U}^{\triangleleft}$ is a linear-depth many-body circuit, this Doob transformation is not locality preserving, i.e., it can map local operators to non-local ones. This property arises from the long-range correlations in ρ^{\triangleleft} . In the past, explicit forms of the (non-trivial) Doob transformation were only explored in limited systems [51] or systems in the hydrodynamic limit [52]. This is because performing the Doob transformation involves a number of challenging steps, including the explicit calculations of the rate function and the left dominant eigenmatrix of a many-body system, as well as taking the matrix square root and inverse of the left dominant eigenmatrix. Thanks to the linear-depth circuit structure of the left dominant eigenmatrix of \mathcal{M}_s in Eq. (SM-34), Eq. (SM-45) provides the first example of a non-trivial many-body Doob channel for arbitrary system sizes, in explicit form.

V. INHOMOGENEOUS TILTING

As discussed in the main text, the spectrum of the tilted channel \mathcal{M}_s features a Jordan block structure so that the system reaches the steady state exactly in L time steps. This structure also allows analysis of a channel where the value of the tilting field s is different on each time step (inhomogeneous tilt).

The inhomogeneous tilted channel for t time steps is

$$\mathcal{M}_{\{s_t\}} = \mathcal{M}_{s_t} \circ \dots \circ \mathcal{M}_{s_2} \circ \mathcal{M}_{s_1} \quad (\text{SM-46})$$

It is convenient to work with the adjoint of this superoperator (note the time-ordering): $\mathcal{M}_{\{s_t\}}^\dagger = \mathcal{M}_{s_1}^\dagger \circ \dots \circ \mathcal{M}_{s_{t-1}}^\dagger \circ \mathcal{M}_{s_t}^\dagger$. The corresponding complementary channel is

$$\widetilde{\mathcal{M}}_{\{s_t\}} = \widetilde{\mathcal{M}}_{s_t} \circ \dots \circ \widetilde{\mathcal{M}}_{s_2} \circ \widetilde{\mathcal{M}}_{s_1} \quad (\text{SM-47})$$

One may verify that this is related to $\mathcal{M}_{\{s_t\}}^\dagger$ by a multiplicative factor and a re-ordering of the time indices.

A. Diagonal initial states

Now use Eq. (SM-38) to obtain the action of this t -fold channel on an arbitrary diagonal basis state of the computational basis:

$$\mathcal{M}_{\{s_t\}}^\dagger \left(P^{(n_0)} \otimes \dots \otimes P^{(n_{L-1})} \right) = \sum_{w_1, \dots, w_t} e^{\sum_i (1-2w_i)s_i} g^\square(w_1, \dots, w_t; n_0, \dots, n_{L-1}) \quad (\text{SM-48})$$

where each variable w_i is summed over $\{0, 1\}$ and similarly every $n_i \in \{0, 1\}$; also

$$g^\square(w_1, \dots, w_t; n_0, \dots, n_{L-1}) = \quad (\text{SM-49})$$

For $t \geq L$ one uses Eqs. (SM-39) and (SM-40) to reduce this to

$$g^\square(w_1, \dots, w_t; n_0, \dots, n_{L-1}) = \quad , \quad (\text{SM-50})$$

which we notice is fully determined by w_1, \dots, w_L ; it is independent of the initial state (n_0, \dots, n_{L-1}) and of (w_{L+1}, \dots, w_t) . Noting the similarity with Eq. (SM-33) and using again Eq. (SM-38), one has from Eq. (SM-48) that

$$\mathcal{M}_{\{s_t\}}^\dagger \left(P^{(n_0)} \otimes \dots \otimes P^{(n_{L-1})} \right) = \mathcal{U}^\triangleleft(m_1 \otimes \dots \otimes m_L) \prod_{t'=1}^L e^{\theta(s_{t'})} \quad (\text{SM-51})$$

Note that this depends on s_1, \dots, s_L via the matrices m_1, \dots, m_L but is independent of n_0, \dots, n_{L-1} (as noted above).

B. Off-diagonal initial states

To characterise in more detail the properties of $\mathcal{M}_{\{s_t\}}^\dagger$ we note that Eq. (SM-51) gives its action on diagonal basis states; we now consider its action on off-diagonal basis states. It is useful to define a folded unitary circuit, acting on a system of $t + L$ qubits,

$$\mathcal{U}^\square = U^\square \hat{\otimes} U^\square :=$$

$$. \quad (\text{SM-52})$$

where U^\square is the corresponding unfolded circuit. The CNOT gate acts as a permutation on computational basis states and this property is inherited by U^\square . This means that

$$U^\square(|w_t, \dots, w_1\rangle \otimes |n_0, \dots, n_{L-1}\rangle) = |q_0, \dots, q_{L-1}\rangle \otimes |b_1, \dots, b_t\rangle \quad (\text{SM-53})$$

where $q_0, \dots, q_{L-1}, b_1, \dots, b_t$ are binary-valued functions of the binary variables $w_1, \dots, w_t, n_0, \dots, n_{L-1}$; note the circuit is rectangular in general so the partitioning of the variables into groups is different for input and output.

Applying $\mathcal{M}_{\{s_t\}}^\dagger$ to an arbitrary off-diagonal basis state, one obtains

$$\mathcal{M}_{\{s_t\}}^\dagger (|n\rangle\langle n'|) = \sum_{w_1, \dots, w_t} e^{\sum (1-2w_i)s_i} \text{Diagram} \quad (\text{SM-54})$$

Recalling (SM-52) and writing Eq. (SM-53) as $U^\square(|w\rangle \otimes |n\rangle) = |q(w, n)\rangle \otimes |b(w, n)\rangle$, we find

$$\mathcal{M}_{\{s_t\}}^\dagger (|n\rangle\langle n'|) = \sum_{w_1, \dots, w_t} e^{\sum_i (1-2w_i)s_i} |q(w, n)\rangle\langle q(w, n')| |b(w, n)\rangle\langle b(w, n')| \quad (\text{SM-55})$$

We now show that this vanishes for $t \geq L$ and $n \neq n'$ which means that $\mathcal{M}_{\{s_t\}}^\dagger(\rho)$ is diagonal for $t \geq L$, as asserted above. Using Eq. (SM-39) with Eqs. (SM-52, SM-53) one sees that if $t \geq L$, then $q(w, n)$ is fully determined by w_1, \dots, w_t ; in particular it is independent of n . Since U^\square is one-to-one (in fact, unitary), this means that $b(w, n') \neq b(w, n)$ unless $n = n'$. Hence for $t \geq L$

$$\mathcal{M}_{\{s_t\}}^\dagger (|n\rangle\langle n'|) = \sum_{w_1, \dots, w_t} e^{\sum_i (1-2w_i)s_i} |q(w, n)\rangle\langle q(w, n)| \delta_{n, n'} \quad (\text{SM-56})$$

which vanishes for off-diagonal initial states, as required. [For $t < L$ and $n \neq n'$ it can be that $b(w, n) = b(w, n')$ because $q(w, n), q(w, n')$ depend on n, n' and may therefore be different.] Eq. (SM-56) is consistent with Eq. (SM-51) on taking $n = n'$; it additionally shows that coherences between computational basis states are destroyed in L steps.

C. Spectrum of \mathcal{M}_s (Jordan blocks)

The results above also establish the Jordan block structure of \mathcal{M}_s . Specifically Eqs. (SM-51) and (SM-56) show that for $t \geq L$ then $\mathcal{M}_{\{s_t\}}^\dagger$ has a single positive eigenvalue and $2^{2L} - 1$ zeros. For the special case where $s_1 = s_2 = \dots = s_t = s$, this means that \mathcal{M}_s^\dagger has a unique non-zero eigenvalue of $e^{\theta(s)}$, but it may generally contain Jordan blocks with sizes less than or equal to L . An argument similar to that of Eq. (SM-50) shows that for $t < L$ the state $g^\square(w_1, \dots, w_t; n_0, \dots, n_{L-1})$ does depend on n_0 ; it follows that the largest Jordan block of \mathcal{M}_s^\dagger has size exactly L . The spectrum of \mathcal{M}_s (and the sizes of its Jordan blocks) are the same as those of \mathcal{M}_s^\dagger .

D. Complementary channel $\widetilde{\mathcal{M}}_s$

Starting from Eq. (SM-47) one also sees [analogous to Eq. (SM-48)] that

$$\widetilde{\mathcal{M}}_{\{s_t\}} \left(P^{(n_0)} \otimes \dots \otimes P^{(n_{L-1})} \right) = \sum_{w_1, \dots, w_t} e^{\sum_i [(1-2w_i)s_i - \theta(s_i)]} g^\square(w_t, \dots, w_1; n_0, \dots, n_{L-1}) \quad (\text{SM-57})$$

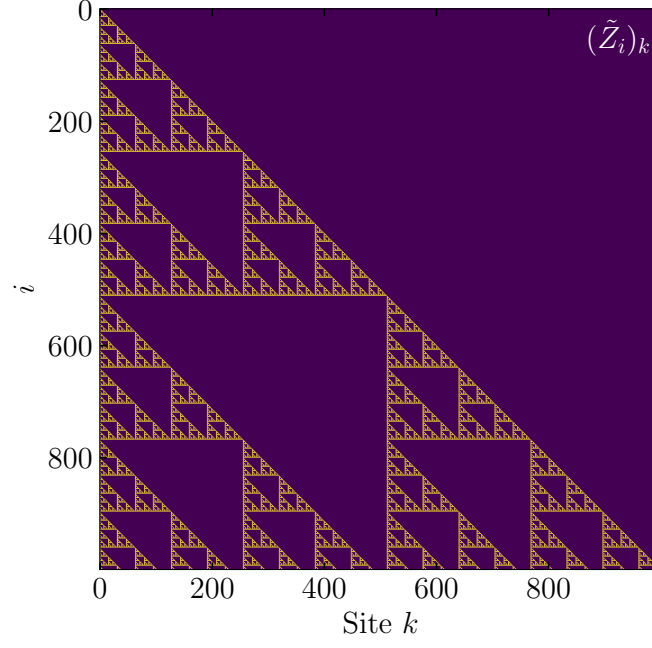


FIG. SM-1. The Pauli-string structure of \tilde{Z}_i for $L = 1000$; The rows plot the component k of string \tilde{Z}_i , where $Z(\mathbf{1})$ is shown in yellow(purple). The emerged Sierpiński triangle is understood using Eq. (SM-66).

It means in particular that if O is a Z string then so is \tilde{O} . We apply Eq. (SM-63) repeatedly to the left hand side of Eq. (SM-62), finding

$$\begin{aligned}
 \mathcal{U}_{\text{SQC}}^{(0)} \left(\bigotimes_{i=0}^{L-1} Z^{z_i} \right) &= \begin{array}{c} \text{Diagram with three blue squares and green circles labeled } z_0, z_{L-3}, z_{L-2}, z_{L-1} \end{array} \\
 &= \begin{array}{c} \text{Diagram with four green circles labeled } \tilde{z}_0, \tilde{z}_{L-3}, \tilde{z}_{L-2}, \tilde{z}_{L-1} \end{array} \quad (\text{SM-64})
 \end{aligned}$$

with $\tilde{z}_i = \oplus_{j=i}^{L-1} z_j$. This is Eq. (SM-62), as required.

A similar result holds for the X Pauli-string, because Z and X are related by a Hadamard matrix. Using the above diagrammatic approach, one arrives at the following

$$\mathcal{U}_{\text{SQC}}^{(0)} \left(\bigotimes_{i=0}^{L-1} X^{z_i} \right) = \bigotimes_{i=0}^{L-1} X^{\oplus_{j=0}^i z_j}. \quad (\text{SM-65})$$

It follows that if O is an X Pauli string then so is \tilde{O} , hence $\langle O \rangle_s$ is zero in that case. Among Pauli strings, only Z strings have finite expectations in Eq. (SM-59). To calculate the expectations in this case we use Eq. (SM-32) to express $\mathcal{U}^\triangleleft$ in terms of the $\mathcal{U}_{\text{SQC}}^{(k)}$'s, and use Eq. (SM-64), as we now discuss.

A. 1-point correlation functions

The simplest non-trivial expectation value for a Z Pauli string is $\langle Z_i \rangle_s$, which we identify as a one-point correlation function. We now show that this correlation function has a *Sierpiński triangle* structure (see Fig. [SM-1](#)), in particular

$$\tilde{Z}_i = \mathcal{U}^\natural(Z_i) = \prod_{k=0}^i Z_k^{\beta_{i,k}}, \quad (\text{SM-66})$$

where

$$\beta_{i,k} = \binom{i}{k} \bmod 2 \quad (\text{SM-67})$$

is the binomial coefficient mod 2. Note that \tilde{Z}_i is a Z Pauli string where all the operators to the right of site i are identities. This means in particular that while the objects in Eq. [\(SM-66\)](#) are L -qubit operators, the equation holds for all $L(> i)$.

A special case of Eq. [\(SM-62\)](#) is that

$$\mathcal{U}_{\text{SQC}}^{(0)}(Z_i) = \prod_{p=0}^i Z_p \quad (\text{SM-68})$$

From [\(SM-31\)](#) the operator $\mathcal{U}_{\text{SQC}}^{(k)}$ acts as the identity on the first k qubits. Repeating the argument leading to Eq. [\(SM-62\)](#) yields the more general result

$$\mathcal{U}_{\text{SQC}}^{(k)}(Z_i) = \begin{cases} \prod_{p=k}^i Z_p & i \geq k \\ Z_i & i < k \end{cases} \quad (\text{SM-69})$$

Using these results with Eq. [\(SM-32\)](#) and unitarity of $\mathcal{U}_{\text{SQC}}^{(k)}$ we have

$$\begin{aligned} \tilde{Z}_i &= \mathcal{U}_{\text{SQC}}^{(L-2)} \cdots \mathcal{U}_{\text{SQC}}^{(1)} \mathcal{U}_{\text{SQC}}^{(0)}(Z_i) \\ &= \mathcal{U}_{\text{SQC}}^{(L-2)} \cdots \mathcal{U}_{\text{SQC}}^{(1)} \left(\prod_{p=0}^i Z_p \right) \\ &= \prod_{p=0}^i \mathcal{U}_{\text{SQC}}^{(L-2)} \cdots \mathcal{U}_{\text{SQC}}^{(1)}(Z_p) \end{aligned} \quad (\text{SM-70})$$

For $i = 0$ this gives $\tilde{Z}_0 = Z_0$ [by Eq. [\(SM-69\)](#)]. For $i > 0$ we have by Eq. [\(SM-69\)](#)

$$\tilde{Z}_i = Z_0 \prod_{p=1}^i \mathcal{U}_{\text{SQC}}^{(L-2)} \cdots \mathcal{U}_{\text{SQC}}^{(1)}(Z_p) \quad (\text{SM-71})$$

The key step is to observe [by the properties of $\mathcal{U}_{\text{SQC}}^{(k)}$ and \mathcal{U}^\natural] that $\mathcal{U}_{\text{SQC}}^{(L-2)} \cdots \mathcal{U}_{\text{SQC}}^{(1)}(Z_p) = \mathbb{1} \otimes \tilde{Z}_{p-1}$ (here \tilde{Z}_{p-1} is interpreted as an operator on $L-1$ qubits, this is consistent because $1 \leq p < L$). Hence

$$\tilde{Z}_i = Z \otimes \prod_{p=1}^i \tilde{Z}_{p-1} \quad (\text{SM-72})$$

We now show Eq. [\(SM-66\)](#) by induction on i . We have shown Eq. [\(SM-66\)](#) for $i = 0$. Fix some i and suppose that

Eq. (SM-66) holds for all $p < i$. Then by Eq. (SM-72) we have

$$\begin{aligned}
\tilde{Z}_i &= Z \otimes \prod_{p=1}^i \prod_{k=0}^{p-1} Z_k^{\beta_{p-1,k}} \\
&= Z_0 \prod_{p=1}^i \prod_{k=0}^{p-1} Z_{k+1}^{\beta_{p-1,k}} \\
&= Z_0 \prod_{k=0}^{i-1} (Z_{k+1})^{\sum_{p=k+1}^i \beta_{p-1,k}} \\
&= Z_0 \prod_{k=0}^{i-1} Z_{k+1}^{\beta_{i,k+1}}
\end{aligned} \tag{SM-73}$$

where the last line uses Fermat's combinatorial identity $\sum_{a=k}^c \binom{a}{k} = \binom{c+1}{k+1}$. The last result is equivalent to Eq. (SM-66), so this concludes the inductive proof.

Using this result with Eqs. (SM-59, SM-61), we obtain

$$\langle Z_i \rangle = \left(\frac{e^s - e^{-s}}{e^s + e^{-s}} \right)^{V_i}, \tag{SM-74}$$

where

$$V_i = \sum_{k=0}^i \beta_{i,k}. \tag{SM-75}$$

is the number of Z operators in the Pauli string \tilde{Z}_i , which is the same as the number of odd numbers in the i th row of Sierpiński's triangle. Hence Eq. (SM-74) is equivalent to Eq. (19) of the main text.

B. 2-point correlation functions

The two point correlation function is

$$\langle Z_i Z_j \rangle_s = \text{Tr} \left[\mathcal{U}^\Delta(\tilde{Z}_i) \mathcal{U}^\Delta(\tilde{Z}_j) m_s^{\otimes L} \right] e^{-L\theta(s)} \tag{SM-76}$$

We consider $i \leq j$ without loss of generality. Using Eq. (SM-66) and that $Z^2 = \mathbb{1}$ we find

$$\mathcal{U}^\Delta(Z_i) \mathcal{U}^\Delta(Z_j) = \bigotimes_{k=0}^i Z^{\beta_{i,k} \oplus \beta_{j,k}}. \tag{SM-77}$$

Using this with Eq. (SM-76) yields

$$\langle Z_i Z_j \rangle_s = \left(\frac{e^s - e^{-s}}{e^s + e^{-s}} \right)^{W_{ij}} \tag{SM-78}$$

where (recall $i \leq j$)

$$W_{i,j} = \sum_{k=0}^i (\beta_{i,k} \oplus \beta_{j,k}) + \sum_{k=i+1}^j \beta_{j,k} \tag{SM-79}$$

is the number of Z operators in the Pauli string $\mathcal{U}^\Delta(Z_i Z_j)$. This is Eq. (20) of the main text.

Introducing the connected correlation function, we have

$$\begin{aligned}
C(i, j) &:= \langle Z_i Z_j \rangle_s - \langle Z_i \rangle_s \langle Z_j \rangle_s \\
&= \left(\frac{e^s - e^{-s}}{e^s + e^{-s}} \right)^{W_{ij}} - \left(\frac{e^s - e^{-s}}{e^s + e^{-s}} \right)^{V_i} \left(\frac{e^s - e^{-s}}{e^s + e^{-s}} \right)^{V_j}.
\end{aligned} \tag{SM-80}$$

We now demonstrate that there are long-range correlations in Eq. (SM-80) by exploring features of the Sierpiński triangle. We make use of Lucas' theorem, which states that $\binom{i}{k} \bmod 2$ is 0 if and only if at least one digit of the binary representation of k is greater than the corresponding digit for i . Hence for integer m , $\binom{2^m-1}{k} \bmod 2$ is 1 for all k ; also $\binom{2^m}{k} \bmod 2$ is 1 if and only if $k = 0, 2^m$. It follows that

$$V_{2^m-1} = 2^m, \quad V_{2^m} = 2 \quad (\text{SM-81})$$

Similarly, for two-point correlations:

$$\begin{aligned} W_{2^m, 2^{m'}} &= 2 \\ W_{2^m-1, 2^{m'}-1} &= 2^{m'} - 2^m \\ W_{2^m, 2^{m'}-1} &= 2^m. \end{aligned}$$

Combining these results yields Eq. (24) of the main text.

A particularly interesting case is $i = 2^m, j = 2^{m'}$, where $W_{i,j}$, V_i and V_j are all equal to 2, independent of m and m' . This means the connected 2-point function Eq. (SM-80) is the same and non-zero for any m and m' . Since $|2^m - 2^{m'}|$ can be arbitrarily large, these are infinite-ranged correlations.

C. Averaged correlations

The correlation function $C(i, j)$ has a complicated dependence on i, j ; the general trend is that larger distances $|i - j|$ correspond to weaker correlations, but there are some special points where the correlation is finite even for very large distances.

To reveal the general trend we consider averages over spatial windows: for any vector $f = (f_0, f_1, \dots)$ we write

$$[f]_a^b = \frac{1}{b-a} \sum_{j=a}^{b-1} f_j \quad (\text{SM-82})$$

where the window is $a \leq j < b$. Also note from the recursive structure of the Sierpiński's triangle that for integers j, m with $j < 2^m$:

$$V_{j+2^m} = 2V_j. \quad (\text{SM-83})$$

Considering the vector (V_0^k, V_1^k, \dots) where we take the k th power of each V_i , this implies

$$\begin{aligned} [V^k]_0^{2^{m+1}} &= \frac{1}{2^{m+1}} \sum_{j=0}^{2^{m+1}-1} V_j^k = \frac{1}{2^{m+1}} \left(\sum_{j=0}^{2^m-1} V_j^k + \sum_{j=0}^{2^m-1} V_{j+2^m}^k \right) \\ &= \left(\frac{1+2^k}{2} \right) [V^k]_0^{2^m} \end{aligned} \quad (\text{SM-84})$$

combining this relation with $[V^k]_0^1 = 1$ we find

$$[V^k]_0^{2^m} = \left(\frac{1+2^k}{2} \right)^m = 2^{m(d_f(k)-1)}. \quad (\text{SM-85})$$

with

$$d_f(k) = \frac{\log(1+2^k)}{\log 2}. \quad (\text{SM-86})$$

1. One-point function

Define $q(s) = \ln \tanh(s)$ as in the main text, we consider $s > 0$ so $q < 0$. We have

$$\langle Z_i \rangle_s = \exp[q(s)V_i] \quad (\text{SM-87})$$

(For $s < 0$ then e^q is real and negative, and q is complex.) Now we compute the one-point correlation function averaged over the window from 0 to 2^m as

$$[\langle Z \rangle_s]_0^{2^m} = \sum_{k=0}^{\infty} \frac{q^k}{k!} [V^k]_0^{2^m} = \sum_{k=0}^{\infty} \frac{q^k}{k!} \left(\frac{1+2^k}{2} \right)^m = \frac{1}{2^m} \sum_{j=0}^m \binom{m}{j} e^{2^j q}, \quad (\text{SM-88})$$

where the last form follows from expanding the binomial and resumming the exponential. This expression can be bounded as follows

$$\frac{1}{2^m} e^{2^m q} \leq [\langle Z \rangle_s]_0^{2^{m-1}} \leq \frac{1}{2^m} \binom{m}{m/2} \frac{e^q}{1 - e^q}, \quad (\text{SM-89})$$

where we took for simplicity m to be even. The lower bound is obtained by only taking the first term in the sum (they are all positive) and the upper bound by setting all binomial coefficients equal to the largest one and using

$$\sum_{j=0}^m e^{2^j q} \leq \sum_{k=1}^{2^m} e^{kq} \leq \frac{e^q}{1 - e^q}. \quad (\text{SM-90})$$

Note that the lower bound in Eq. (SM-89) scales as 2^{-m} and since

$$\frac{1}{2^m} \binom{m}{m/2} = \sqrt{\frac{2}{m\pi}} + O\left(\frac{1}{m^{3/2}}\right), \quad (\text{SM-91})$$

the upper bound scales like $m^{-1/2}$.

Finally we consider a sequence of system sizes that are powers of two ($L = 2^p$) and average the one-point function over the whole system to bound the averaged correlation

$$C_1 < [\langle Z \rangle_s]_0^L < C_2, \quad C_1 \sim L^{-1}, \quad C_2 \sim (\log L)^{-1/2} \quad (\text{SM-92})$$

This upper bound shows that $[\langle Z \rangle_s]_0^L$ decays with L ; the lower bound shows that this decay is no faster than a power law.

2. Two-point function

The two point function can be treated in a similar way. We consider the illustrative case $i = 2^m \leq j$ for which

$$\langle Z_i Z_j \rangle_s = \langle Z_j \rangle_s \exp[-2q\beta_{j,i}] \quad (\text{SM-93})$$

where we used that $\beta_{j,0} = 1$. It is also useful to note that Lucas's theorem implies

$$\beta_{j,2^m} = j_m, \quad (\text{SM-94})$$

where j_m is the m -th coefficient of the expansion of j in base 2. This means that we can write the following window-averaged correlation:

$$[\langle Z_{2^m} Z_j \rangle_s]_{2^n}^{2^{n+1}} = \frac{1}{2^n} \left(\sum_{k=0}^{2^{n-m-1}-1} \sum_{a=0}^{2^m-1} \langle Z_{2^n+a+2^m(2k+1)} \rangle_s + e^{-2q} \sum_{k=0}^{2^{n-m-1}-1} \sum_{a=0}^{2^m-1} \langle Z_{2^n+a+2^{m+1}k} \rangle_s \right). \quad (\text{SM-95})$$

To simplify this expression, we introduce the (m -dependent) parity-split window averages of f

$$[f']_{2^n}^{2^{n+1}} := \frac{1}{2^n} \sum_{k=0}^{2^{n-m-1}-1} \sum_{a=0}^{2^m-1} f_{a+(2k+1)2^m+2^n}, \quad [f'']_{2^n}^{2^{n+1}} := \frac{1}{2^n} \sum_{k=0}^{2^{n-m-1}-1} \sum_{a=0}^{2^m-1} f_{a+(2k)2^m+2^n}, \quad (\text{SM-96})$$

such that

$$[f]_{2^n}^{2^{n+1}} = [f']_{2^n}^{2^{n+1}} + [f'']_{2^n}^{2^{n+1}}. \quad (\text{SM-97})$$

Proceeding inductively by analogy with the derivation of Eq. (SM-85) we find

$$[V^{k'}]_{2^n}^{2^{n+1}} = \left(\frac{2^{2k}}{1+2^k} \right) \left(\frac{1+2^k}{2} \right)^n, \quad [V^{k''}]_{2^n}^{2^{n+1}} = \left(\frac{2^k}{1+2^k} \right) \left(\frac{1+2^k}{2} \right)^n, \quad [V^k]_{2^n}^{2^{n+1}} = 2^k \left(\frac{1+2^k}{2} \right)^n. \quad (\text{SM-98})$$

Despite the dependence of the window-split average on m , it is important here that all these objects are independent of this parameter, which is due to Eq. (SM-83). Using the results above we then have

$$\begin{aligned} [\langle Z_{2^m} Z \rangle_s]_{2^n}^{2^{n+1}} &= \sum_{p=0}^{\infty} \frac{q^p}{p!} \left(\frac{2^{2p}}{1+2^p} \right) \left(\frac{1+2^p}{2} \right)^n + e^{-2q} \sum_{p=0}^{\infty} \frac{q^p}{p!} \left(\frac{2^p}{1+2^p} \right) \left(\frac{1+2^p}{2} \right)^n \\ &= \frac{1}{2^n} \sum_{j=0}^{n-1} \binom{n-1}{j} e^{2^{j+2}q} + \frac{e^{-2q}}{2^n} \sum_{j=0}^{n-1} \binom{n-1}{j} e^{2^{j+1}q}, \end{aligned} \quad (\text{SM-99})$$

and analogously [cf. Eq. SM-88]

$$[\langle Z \rangle_s]_{2^n}^{2^{n+1}} = \sum_{p=0}^{\infty} \frac{(2q)^p}{p!} \left(\frac{1+2^p}{2} \right)^n = \frac{1}{2^n} \sum_{j=0}^n \binom{n}{j} e^{2^{j+1}q}. \quad (\text{SM-100})$$

Finally putting all together, we obtain an expression for the window-averaged two-point function and $i = 2^m$

$$[\langle Z_i Z \rangle_s - \langle Z_i \rangle_s \langle Z \rangle_s]_{2^n}^{2^{n+1}} = \frac{1}{2^n} \sum_{j=0}^{n-1} \binom{n-1}{j} \left[e^{2^{j+2}q} - 2 \sinh(2q) e^{2^{j+1}q} \right] + e^{2q} \frac{e^{2^{n+1}q}}{2^n}. \quad (\text{SM-101})$$

Similar to Eq. (SM-88), this expression can be bounded to show that the correlations decay with n (no faster than algebraically, note $\sinh(2q) < 0$), see the main text for a discussion. The fact that the RHS is independent of m shows that the decay of these correlations is controlled by the distance of the rightmost site from the origin, instead of by the distance between sites i, j .